COBEM 2023 27TH INTERNATIONAL CONGRESS OF MECHANICAL ENGENEERING

ABCM Brazilian Society of Mechanical Sciences and Engineering
27th ABCM International Congress of Mechanical Engineering
December 04-08, 2023, Florianópolis-SC, Brazil

COB-2023-0285
Evolutionary Topology Optimization of Pressure-actuated Compliant Mechanisms

Vitor Hugo Lopes Costa Lima
Claudia Marcela Perez Madrid
Heitor Nigro Lopes
Daniel Candeloro Cunha
Renato Pavanello
Faculdade de Engenharia Mecânica - Universidade Estadual de Campinas. R. Mendeleyev, 200 - Cidade Universitária, Campinas, SP, Brazil. Zip-code: 13083-860
v203969@dac.unicamp.br
c151692@dac.unicamp.br
lopes@fem.unicamp.br
cunha@fem.unicamp.br
pava@fem.unicamp.br

Abstract. *Compliant Mechanisms (CM) transmit movement without mechanical joints and use body deformation to achieve motion. In some applications, the CMs are fluid-actuated for what they are called Pressure-actuated Compliant Mechanisms (Pa-CM). This work used topology optimization to optimize the Pa-CMs structure by considering dependent loads to represent the fluid pressure. The Bidirectional Evolutionary Structural Optimization (BESO) method is adopted for this case, given that it uses discrete design variables. This discrete method allows well-defined geometric boundaries between solid and void for the structure. To include the design-dependent load problem, it was necessary to establish a new sensitivity analysis to determine the load influence over the structure and perform the mechanisms optimization. First, CM structures were optimized, leading to topologies similar to those reported in the literature. Then, the optimization of Pa-CM presented different compared to results found in previous works for benchmark Pa-CMs cases. A virtual flux method restriction was implemented to prevent unpredictable changes in the topology caused by the combination of fluid elements and large void regions already generated. The BESO found well-defined structures, considering dependent loads in the formulation. The virtual flux method showed potential applications for the improvement of the overall connectivity of the final topologies.*

Keywords: *BESO, Design Dependent Loads, Pa-CM, Virtual Flux Method*

1. INTRODUCTION

Compliant Mechanisms (CMs) transmit movement without flexion joints or sliding parts, its bending deformation produces useful work. Consequently, these mechanisms have reduced looseness and wear, besides their high precision (Howell *et al.*, 2013). CMs have many applications and may be found in many daily mechanisms. These devices have employment in soft robots, which are tools used in useful and complex applications, such as the substitution of human organs, surgical equipment, and manipulation of extremely fragile objects (Yap *et al.*, 2016; Chen *et al.*, 2018). CMs have many means of actuation, one of them, approached in this work, is the actuation by fluid. CMs actuated by fluid pressure characterize Pressure-actuated Compliant Mechanisms (Pa-CMs).

The advances in computational processing and additive manufacturing allow the synthesis and building of new and complex CMs. One of the methods used to find new or optimal CMs structures is structural optimization, such as Topology Optimization (TO). Many studies optimizing CMs with TO have been carried out in literature involving many actuation problems, applications, and TO methods (Zhu *et al.*, 2020). Recently, there has been an increasing interest in TO of Pa-CMs (Cunha, 2019; de Souza and Silva, 2020; Kumar *et al.*, 2020; Kumar and Langelaar, 2021; Lu and Tong, 2021; Kumar and Langelaar, 2022). Except for Cunha (2019) and de Souza and Silva (2020), the mentioned works used TO methods that interpolate the structural stiffness using continuum variables. This approach allows the presence of gray elements between void and solid, which requires a secondary strategy to remove them from the design domain. The Bi-directional Evolutionary Topology Optimization (BESO) uses discrete design variables to represent the topology, allowing a well-defined interface between fluid and solid elements.

This work aims to carry out the topology optimization of Pa-CMs using BESO. The first part describes some CM optimization cases to test the objective function of this method. Then, some Pa-CMs mechanisms examples from Kumar and Langelaar (2022) are optimized to verify the implemented method. Finally, a modified Virtual Flux Method, based on

the original VFM described in Lopes *et al.* (2022), is implemented and tested on the optimization of Pa-CMs, by avoiding big changes in the topology evolution.

2. BI-DIRECTIONAL EVOLUTIONARY STRUCTURAL OPTIMIZATION

The BESO method is an improvement of the Evolutionary Structural Optimization (ESO) (Xie and Steven, 1992), which is defined by a discrete method, where solid elements ($x = 1$) of a finite element mesh can be switched to void ($x = x_{min}$), and vice versa, to maximize an objective function $h(x)$ (Huang and Xie, 2010). Here, the void elements are represented by x_{min} because material interpolation is utilized as a way to avoid singularity problems on the solution to the finite element problem. This way, the global stiffness matrix $\mathbf{K}$ of the structure is defined by $\mathbf{K^0}$ and pseudo-density (x_e):

$$\boldsymbol{K} = \sum_e x_e^p \boldsymbol{K}_e^0 \tag{1}$$

Where the term p is a penalty exponent which in plane stress problems has a value of 3. Normally, $x_{min} = 0.001$.

To define if an element must be turned into void or solid a sensitivity analysis is done. The sensitivity number of each element (α_e) is defined as an approximation of how the objective function varies with the fluctuation of the pseudo-density of one element.

$$\alpha_e = \frac{\partial h(x_e)}{\partial x_e} \tag{2}$$

By calculating the sensitivity distribution, ordering the α for solid and void elements, it's possible to find the solid elements which $\alpha_e \leq \alpha_{del}$, to become void, and void elements which $\alpha_e \geq \alpha_{add}$, to become solid. The terms α_{del} and α_{add} may be found using the predefined parameters ER and AR. The first is the Evolutionary Ratio, which assigns how much of the volume is decreased each iteration, and the second is the Addition Ratio, which states how many of the void elements are added again. In general, a target volume V^* is defined to state when to stop removing elements, then the optimization continues until a convergence criterion is met.

Because the BESO is a discrete method, a filter scheme must be used to avoid checkerboard, one-node connection, and mesh dependence. This filter works by recalculating α_e by making a weighted average of the sensitivity number of the nodes inside a circle with a radius of r_{min} from the center of element e. The nodal sensitivity is calculated by averaging the sensitivity number of the elements connected with the node.

3. COMPLIANT MECHANISMS OPTIMIZATION

As a way of defining the optimization problem, an objective function must be maximized. Li (2014) optimized CMs with BESO, comparing objective functions, including the $h(x) = GA/SE$, which was formulated as a method to generate hinge-free CMs, where GA is defined as the geometric advantage and SE is a measure of the CM strain energy. However, Li (2014) used a modified BESO, where the pseudo-densities assumed intermediaries values between 0 and 1. Because of that, this formulation was repeated in a later work more detailed in Madrid (2016) with a discrete BESO. However, to perform the optimization of Pa-CMs, the objective function $h(x) = GA/SE$ cannot be used since the term GA is a function of just one input port displacement u_{in}. In a distributed load problem, there are numerous input spots, so this function is not suitable for this problem. Therefore, another objective function was tested to carry out the optimization of simple actuated CMs using the discrete BESO. The first part of this work describes the BESO optimization of simple CM with the objective function MSE/SE, which was first used for topology optimization of CMs in Frecker *et al.* (1997).

3.1 MSE/SE formulation

The MSE/SE formulation is characterized by the objective function in Eq. 3:

$$h(x) = \frac{MSE}{SE} \tag{3}$$

Where MSE is the Mutual Strain Energy and the SE term is the Strain Energy. These terms are determined by solving a linear system with boundary conditions as illustrated in Fig. 1. A force F_{in} is applied in the input port, causing a displacement u_{in} on that degree of freedom. On the output degree of freedom, the u_{out} displacement is generated. A virtual spring, which adds a stiffness k_{out} in the global stiffness $\mathbf{K}$, is placed to cause a reaction force F_{out} on this point.

The MSE evaluates output displacement by applying a dummy load on the output port:

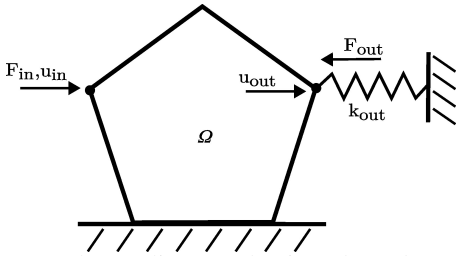

Figure 1: General compliant mechanisms boundary conditions.

$$MSE = \mathbf{\Lambda_{out}}^T \mathbf{K} \mathbf{U} \tag{4}$$

Where $\mathbf{\Lambda_{out}}$ is the displacement caused by a dummy unitary force applied on the output port, on the desired output displacement direction, $\mathbf{L_{out}}$, and $\mathbf{U}$ is the displacement vector caused by the force applied in the input port $\mathbf{F}$. Since $\mathbf{L_{out}}$ is unitary on the output degree of freedom and zero on the others, the value of MSE will be equivalent to the output degree of freedom displacement. The system $\mathbf{KU} = \mathbf{F}$ has to be solved to find $\mathbf{U}$.

SE evaluates how much of the energy is absorbed by the structure, and is used as a measure of structure flexibility. Also, the energy of the virtual spring must be subtracted from the strain energy. Therefore, SE can be calculated as:

$$SE = \frac{1}{2}\mathbf{U}^T\mathbf{K}\mathbf{U} - k_{out}MSE^2 \tag{5}$$

3.1.1 Sensitivity Analysis

To find the sensitivity number of the elements, the derivative of the objective function has to be calculated as in Eq. 6. For this, both terms $\frac{\partial MSE}{\partial x_e}$ and $\frac{\partial SE}{\partial x_e}$ must be found.

$$\alpha_e = \left(SE\frac{\partial MSE}{\partial x_e} - MSE\frac{\partial SE}{\partial x_e} \right) / SE^2 \tag{6}$$

Starting with $\frac{\partial MSE}{\partial x_e}$, because of the relation $\mathbf{K\Lambda_{out}} = \mathbf{L_{out}}$, $MSE = \mathbf{L_{out}}^T\mathbf{U}$. By differentiating MSE, $\mathbf{L_{out}}$ is independent of the topology, and its derivative is zero. Equation 7 is found.

$$\frac{\partial MSE}{\partial x_e} = \mathbf{L_{out}}^T \frac{\partial \mathbf{U}}{\partial x_e} \tag{7}$$

$\frac{\partial \mathbf{U}}{\partial x_e}$ can be easily found by deriving $\mathbf{KU} = \mathbf{F}$. Considering the material interpolation, the derivative of the elemental stiffness matrix is determined:

$$\frac{\partial \mathbf{K_e}}{\partial x_e} = p x_e^{(p-1)} \mathbf{K}_e^0 \tag{8}$$

Where $\mathbf{K}_e^0$ is the solid element stiffness matrix. Then the term $\frac{\partial MSE}{\partial x_e}$ is found for each element e.

$$\frac{\partial MSE}{\partial x_e} = -p x_e^{(p-1)} \mathbf{\Lambda_{out}}^T \mathbf{K_e^0} \mathbf{U_e} \tag{9}$$

The term $\frac{\partial SE}{\partial x_e}$ can be found deriving the expression.

$$SE = \frac{1}{2}\mathbf{F}^T\mathbf{U} + \lambda^T(\mathbf{F} - \mathbf{KU}) - k_{out}MSE^2 \tag{10}$$

Which includes a Lagrange multiplier, λ, to help the solution. The derivative of the force $\mathbf{F}$ becomes 0 because it is independent of the topology. Using $\lambda = \frac{1}{2}\mathbf{U}$, it is found that:

$$\frac{\partial SE}{\partial x_e} = -\frac{1}{2} p x_e^{(p-1)} \left(\mathbf{U_e}^T \mathbf{K_e^0} \mathbf{U_e} \right) - 2k_{out} MSE \frac{\partial MSE}{\partial x_e} \tag{11}$$

Adopting Eq. 9 and Eq. 11 the sensitivity number α_e in Eq 6 of each element may be calculated.

3.2 Optimization Results

Some examples were considered to evaluate the method implemented, and each boundary condition and its final topology are described next. All of the mechanisms were optimized, starting with a full design domain. The algorithm used linear elastic materials and a 2D mesh with plane stress conditions. Just one-half of the design domains illustrated were modeled considering symmetry. More details of the optimization parameters may be verified in Madrid (2016).

3.2.1 Inverter Mechanism

The inverter mechanism is characterized by the output displacement direction being opposite to the input force. Figure 2 illustrates the boundary conditions for this mechanism and the final topology after optimization using a mesh of 200×100 elements.

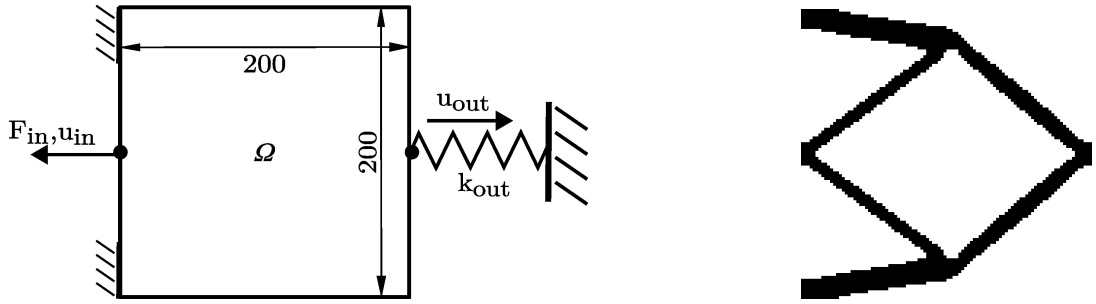

(a) (b)

Figure 2: (a) Boundary conditions of inverter mechanism. (b) Inverter topology optimized.

3.2.2 Inverted Gripper Mechanism

The inverted gripper is a mechanism where the actuation force pulls the input port causing a displacement on two output ports, making the structure close a gap in this region, making a grasping movement. So the movement of the output port has to be inverted from the initial movement when the design domain is full. Figure 3 shows the boundary conditions of the mechanism and the optimization result.

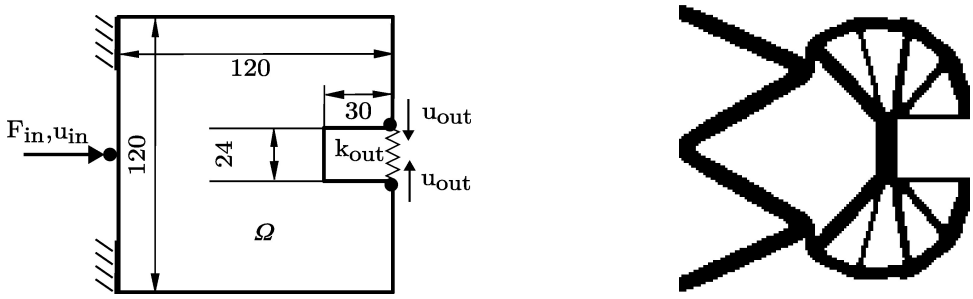

(a) (b)

Figure 3: (a) Boundary conditions of inverted gripper mechanism. (b) Inverted gripper topology optimized.

3.3 Optimization Curves

Figure 4 illustrates the evolution of the topology, objective function, and volume throughout the BESO iterations for the inverter mechanism, as an example. The volume decreases until it reaches the target volume V^*, at this point the objective functions vary little compared with the rest of the iterations. As the other mechanisms, the objective function increases in the first iterations until it finds its maximum value, then it starts to fall. This happens, because when the $h(x)$ finds its maximum, MSE finds its maximum, and then it changes little, until convergence. From this point objective function falls because the SE continues to increase, since the amount of material reduces every iteration, and the structure gets more and more flexible, independently if maximizing $h(x)$ reduces SE. This behavior happens even in the Pa-CM optimization, which are described in the next section.

For the case where the desired output displacement is in the opposite direction of the displacement in the first iteration, like the inverter and the inverted gripper mechanisms, the optimization removes elements from the output port neighborhood. As illustrated in Fig. 4, in the first iterations the objective function goes to zero, because elements are removed

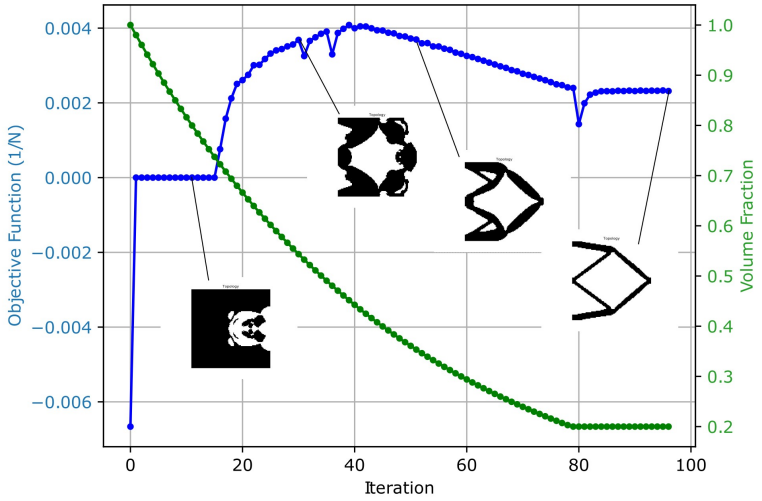

Figure 4: Evolution curves of BESO optimization for inverter mechanism.

around the output port. This happens because the algorithm tends to go with the most feasible topology solution to make the displacement go the opposite way: make it zero. Despite this, at some point, the optimization method adds material in this region again.

3.4 CM optimization final considerations

The final topologies of the mechanisms are very similar to those found in the literature. The methodology followed in the beginning was to use the same parameters reported in Madrid (2016), however, some of these parameters (k_{out}, ER, AR and r_{min}) had to be modified to make the optimization more stable. For all of the mechanisms, the value of k_{out} had to be increased from 10^9 N/m onwards.

4. PRESSURE-ACTUATED COMPLIANT MECHANISMS OPTIMIZATION

Now considering a mechanism actuated by fluid pressure as illustrated by Fig. 5a. The mechanism has the solid domain (Ω_s) and fluid domain (Ω_f). The solid domain has displacement restriction $\mathbf{u_0}$ on S_u. The pressure $\mathbf{P_{in}}$ is applied on S_p portion, on the fluid domain, and produces a u_{out} displacement on the output port. The fluid-structure interface is defined by S_{fs} and $\mathbf{n}$ is the normal vector to S_{fs}.

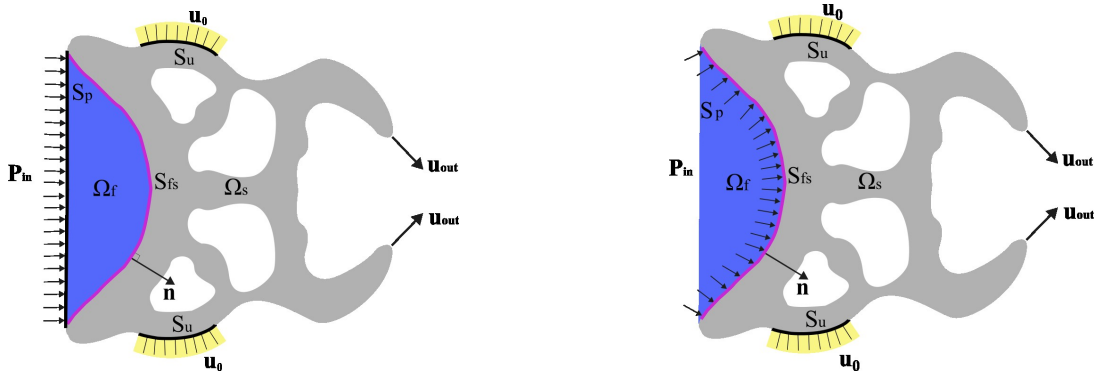

Figure 5: Pressure-actuated compliant mechanism boundary conditions. Gray represents solid domain, blue represents fluid domain, white represents void, pink represents fluid-solid interface, and yellow represents displacement restrictions. (a) Fluid-structure model. (b) Dependent load model.

In this work, the pressure is applied directly on the S_{fs} interface in $\mathbf{n}$ direction, as shown in Fig. 5b. Then, the model used in this work is a design dependent load problem, the application of the load depends on the topology. Every time solid material in contact with the S_{fs} interface is turned into void, it becomes a fluid element, and S_{fs} is updated with solid neighbor elements. This is how S_{fs} changes through optimization. At the beginning of the optimization, there is no fluid element and $S_p = S_{fs}$, where the load is applied. As soon as elements are removed, the fluid domain starts to be formed.

4.1 Sensitivity Analysis with Dependent Load

Since the load is design dependent, some simplifications done to the sensitivity analysis of simple CM cannot be applied here. Now the derivative $\frac{\partial \mathbf{F}}{\partial x_e} \neq 0$. To find this value, it's utilized a linear approximation of Yang *et al.* (2005), where the force vector variation can be approximated as when a single element is removed, $\frac{\partial \mathbf{F}}{\partial x_e} = \Delta F$. Figure 6a shows a small example of the load (pink arrows) applied by a fluid element in solid elements during iteration k. In the next iteration, k + 1, when one of the solid elements in contact with the fluid is removed and becomes a fluid element, another load pattern is applied to the solid elements as shown in Fig.6b. Taking the force vector for both iterations, it is found the variation of the force due to the removal of the solid element, ΔF.

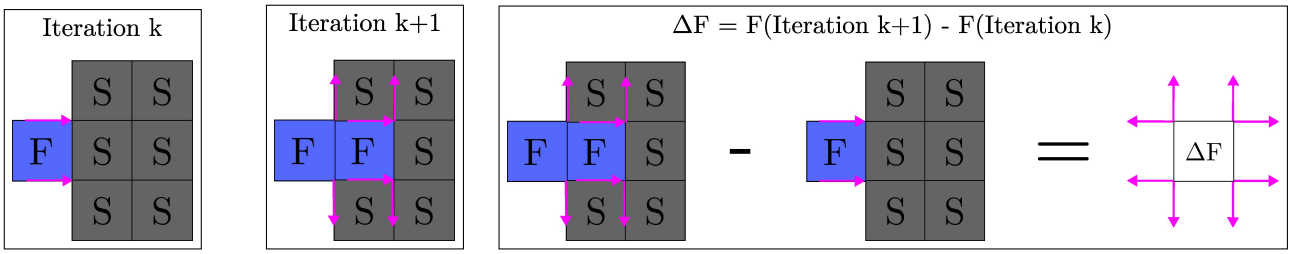

(a) (b) (c)

Figure 6: Illustration of linear force vector variation, $\mathbf{\Delta F}$ for one element shifting. (a) Iteration before solid element shifting. (b) Iteration after solid element shifting. (c) Approximation for $\mathbf{\Delta F}$ based on solid element shifting into fluid element.

The expression for $\frac{\partial MSE}{\partial x_e}$ is the same as shown in Eq. 7 since $\mathbf{L_{out}}$ is still independent of the topology, but the term $\frac{\partial \mathbf{U}}{\partial x_e}$ must be recalculated by differentiating $\mathbf{KU} = \mathbf{F}$ and keeping the term $\frac{\partial \mathbf{F}}{\partial x_e}$. Considering material interpolation, Eq. 12 gives a new expression to $\frac{\partial MSE}{\partial x_e}$.

$$\frac{\partial MSE}{\partial x_e} = \mathbf{\Lambda_{out}}^T \left(\frac{\partial \mathbf{F}}{\partial x_e} - \mathbf{U} \frac{\partial \mathbf{K}}{\partial x_e} \right) = p x_e^{(p-1)} \mathbf{\Lambda_{out}}^T \left(\mathbf{\Delta F} - \mathbf{K_e^0 U_e} \right) \tag{12}$$

The expression for $\frac{\partial SE}{\partial x_e}$ may be found by differentiating the Eq. 10 and using again $\lambda = \frac{1}{2}\mathbf{U}$.

$$\frac{\partial SE}{\partial x_e} = -\frac{1}{2} p x_e^{(p-1)} \mathbf{U_e}^T \left(\mathbf{\Delta F} - \mathbf{K_e^0 U_e} \right) - 2 k_{out} MSE \frac{\partial MSE}{\partial x_e} \tag{13}$$

4.2 Virtual Flux Method (VFM)

In problems involving dependent loads, the sensitivity analysis cannot predict what happens to the objective function when a large region connected to the pressure fluid is removed, since its approximation evaluates the changes by removing one element. This becomes a problem when the fluid domain connects to a region with a large void region, where all the void elements become fluid. The load applied changes completely and the way the optimization follows is unknown. To solve this problem, it was implemented a method to prevent the fluid to connect with void regions already created.

The VFM is a restriction method based on the calculation of the heat flux in a solid structure, to penalize the sensitivity analysis according to connectivity restrictions. This method is based on the VTM (Virtual Temperature Method) of Liu *et al.* (2015), which was proposed to prevent void regions inside the structure. The original VFM, proposed in Lopes *et al.* (2022) has the objective of avoiding disconnection between important parts of the structure. Here, the VFM was modified to prevent the fluid region to connect to void region formed in previous iterations.

The method works by defining a secondary system to be solved, a conduction finite element problem. The problem considers the topology of the current iteration, where fluid elements get a temperature $T_{hot} = 1$ and void elements get a temperature $T_{cool} = 0$, as illustrated in Fig.7. This simple finite element conduction problem can be solved to find the heat flux q_e through the solid elements. As void elements get closer to fluid elements, the heat flux through the wall between them increases. By defining a q_{max}, it's possible to increase the sensitivities of the elements of this region, to prevent their removal.

The q_{max} is approximated by considering an infinite linear wall, with L_{min} thickness, where the temperature gradient and the conductivity coefficient are both 1, then $q_{max} = \frac{1}{L_{min}}$.

The sensitivity number may be recalculated by a $c(q_e)$ parameter defined as:

$$c(q_e) = \begin{cases} \left(\frac{q_e}{q_{max}} \right) & \text{when: } q_e < q_{max} \\ 1 & \text{when: } q_e \geq q_{max} \end{cases} \tag{14}$$

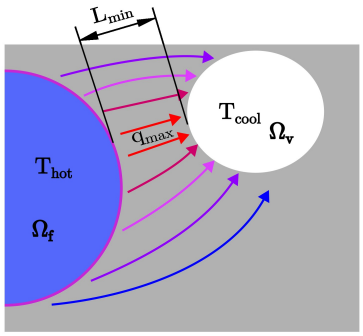

Figure 7: Illustration of VFM's heat flux of wall thickness restriction.

The restriction is made by calculating the new sensitivity analysis α_e^c:

$$\alpha_e^c = \alpha_e + c(q_e)\,[max(\alpha) - \alpha_e] \tag{15}$$

Then, when the heat flux of an element gets close to q_{max}, its sensibility number is increased.

4.3 Pa-CM Results

The implemented method was analyzed with three mechanisms reported by Kumar and Langelaar (2022): the inverter, gripper, and contractor. Most of the optimization parameters were repeated from Kumar and Langelaar (2022), such as material (Young's modulus of 3 GPa e Poisson's coefficient of 0.4), boundary conditions (P_{in} = 1bar and, S_u length of 2mm for gripper and inverter mechanisms and S_u length of 5mm for contractor mechanism). The mechanisms were modeled with one-half by considering symmetry in the vertical direction (with mesh 200×100), with the exception of the contractor, which was modeled only one-fourth using symmetry in both directions (with mesh 100×100). The x and y full length were set to 0.2m and 0.2m, respectively, and the thickness was set to 0.001m. The ER and AR were both set at 1%. The filter radius parameter was set to $r_{min} = 2.5$mm. The final volume restriction was set $V^* = 20\%$. k_{out} was set to 1×10^{11} N/m. In order to compare the topologies with Kumar and Langelaar (2022), the output displacements of the final topologies were calculated with a virtual spring with $k_{out} = 1 \times 10^4$. The results are presented bellow.

4.3.1 Pressure-actuated Inverter Mechanism

Figure 8 illustrates the boundary condition for the inverter mechanism and its final topology.

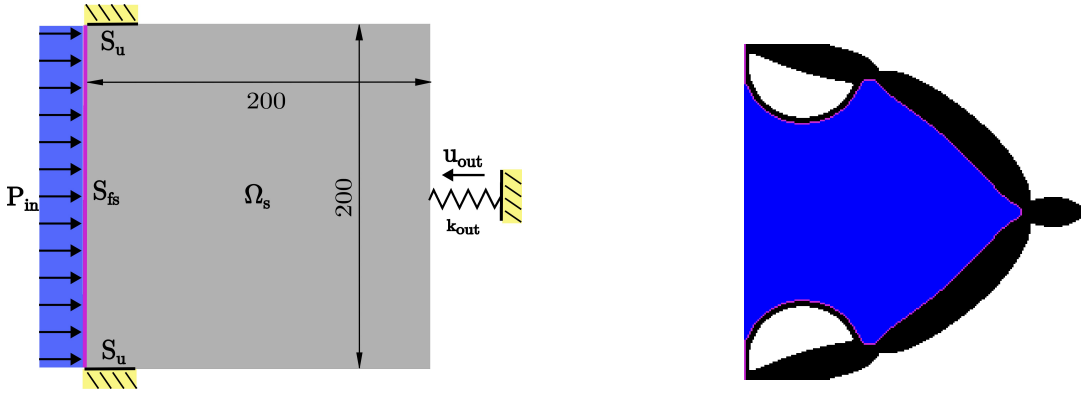

(a) (b)

Figure 8: (a) Boundary conditions of pressure-actuated inverter mechanism. (b) Pressure-actuated inverter optimized topology.

The topology is similar to some topologies found in Kumar and Langelaar (2022). Its displacement in the output port is 0.34mm. The topology forms some bubbles shapes which provide vertical pressure, making half of the bars go up and pulling the output port backward. Regarding the topology evolution, the optimization starts by removing elements from the output port region, but after 35 iterations it adds material back there, and the mechanism starts to take shape in a stable curve.

4.3.2 Pressure-actuated Gripper Mechanism

As the inverted gripper mechanism, the gripper mechanism has to make a grasping movement with the load applied. Figure 9 shows the boundary conditions applied and the optimized topology.

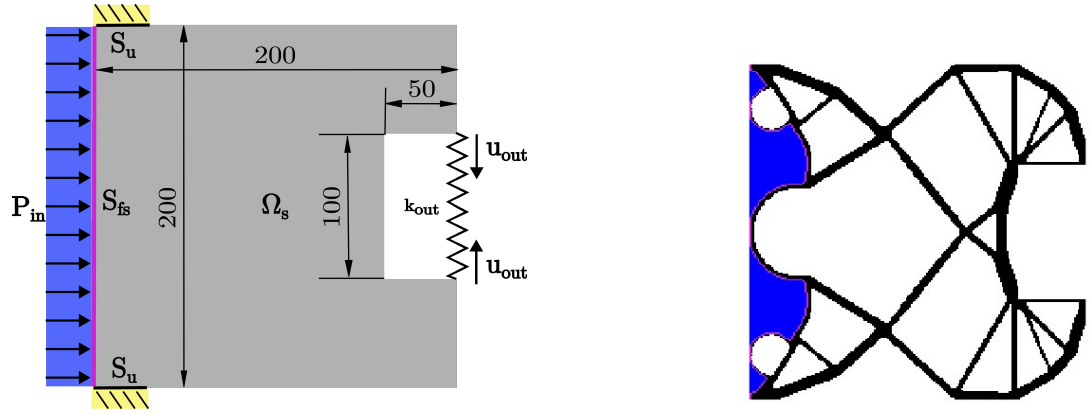

(a) (b)

Figure 9: (a) Boundary conditions of pressure-actuated inverter mechanism. (b) Pressure-actuated inverter optimized topology.

The topology is very different from those reported by Kumar *et al.* (2020), Kumar and Langelaar (2022), and Lu and Tong (2021), even though most of the parameters were kept the same. The displacement of the output port is 0.44mm, which is a value higher than the displacements reported by Kumar and Langelaar (2022). The evolution of the objective function is smoother than the inverter curve. In the beginning, the optimization removes material from the output region but adds back material in the output port after 7 iterations.

4.3.3 Pressure-actuated Contractor Mechanism

Figure 10 illustrates the boundary condition and optimized topology for the contractor mechanism. This mechanism is pressure actuated by the left and right and has to perform a vertical contraction movement in two output ports towards its center region.

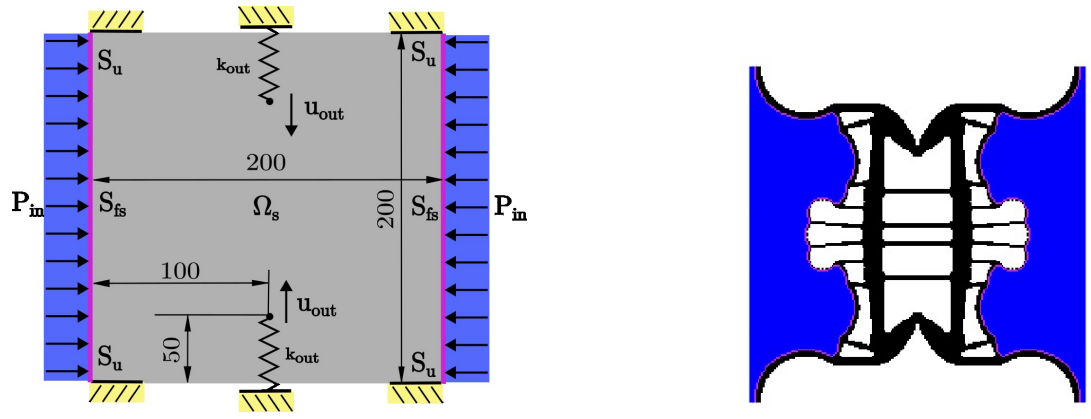

(a) (b)

Figure 10: (a) Boundary conditions of pressure-actuated contractor mechanism. (b) Pressure-actuated contractor optimized topology.

Even though the optimization gets to find a final contractible topology, the optimization is very unstable, the support gets continuously removed from the topology, and the objective function goes to zero. Even in this final topology found, it has fragile support. The found topology is very different from those found in Kumar and Langelaar (2022). Yet, it reaches a displacement of 0.12mm, a value near to the value in the literature. Since the optimization is unstable, the evolution curves are very irregular.

4.4 VFM Influence

Figure 11 illustrates the topologies of the previous mechanisms optimized again, with the VFM.

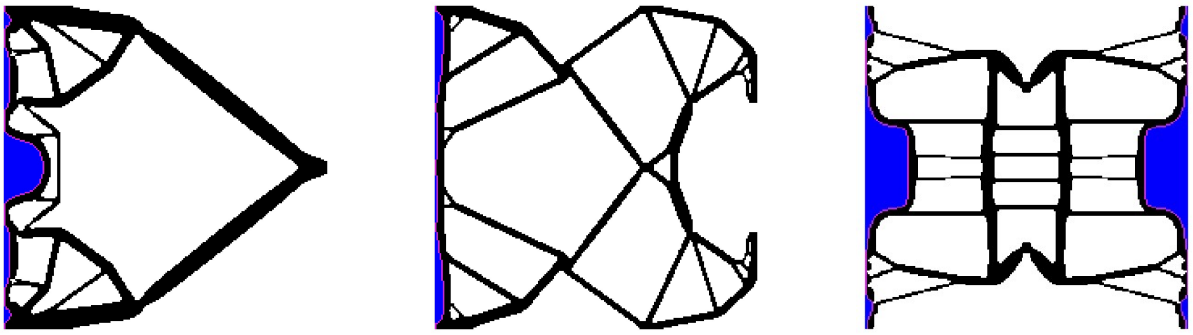

(a) (b) (c)

Figure 11: (a) Pressure-actuated inverter mechanism topology with VFM. (b) Pressure-actuated gripper mechanism topology with VFM. (c) Pressure-actuated contractor mechanism topology with VFM.

The inverter mechanism shown in Fig. 11a appears to be very affected by the VFM. The VFM is successful on preventing the fluid from joining the big void region inside the mechanism. The optimization with the VFM found a topology with a displacement in the output of 0.38mm, which is slightly bigger than the displacement of Fig. 8. The topology illustrated in Fig. 11b found an output displacement similar to the previous optimization, even though the topologies are different. The VFM was able to stabilize the contractor mechanism optimization, but the final topoloy seems to be very fragile, since it formed some thin bars, acheaving an output displacement of 0.08mm.

In general, it was observed that the VFM helped to prevent the fluid from connecting with void regions and still generate feasible topologies. However, some drawbacks appeared due to this method. Thinner bars are formed because the optimization tends to keep material in the region between fluid and void regions. Also, this method works by only holding the fluid-void barriers that are formed when the fluid gets close to some void.

4.5 Pa-CM Discussion

The results with the optimized Pa-CM showed that the BESO was able to find effective topologies, though very unstable in the case of the contractor. The displacements found in the first tests with this algorithm are higher in comparison to works in the literature, even though mesh, boundary conditions, and materials were set the same. It is suitable to compare the topologies found in this work and those reported in the Kumar and Langelaar (2022) because the inverter topology (Fig. 8) has an output displacement very close to the displacements of similar topologies of Kumar and Langelaar (2022). The evolution curves of the optimizations are very similar to what is shown in Fig. 4.

The modified VFM, still new and unexplored, showed satisfactory results by influencing the final topology. It found different topologies by keeping a "wall" thickness every time the fluid region got close to void regions. However, this method still needs some improvements in order to allow an evolution of the topology in the "wall" throughout the optimization. Thus the problem of generating thin bars to keep the connection of the structure with this "wall", would be solved.

5. CONCLUSION

This work applied the BESO method to perform topology optimization of compliant mechanisms. In the first part, it was tested an objective function still not used with discrete BESO in CMs. After successful optimization, with well-known topologies found, the optimization was applied to pressure-actuated CMs. The optimization of Pa-CMs also found feasible topologies, some different and some similar to examples already found in the literature. The next steps are to explore the optimization of other types of Pa-CM and evaluate the influence of the BESO parameters on the final topology.

A restriction method based on virtual heat flux, modified VFM, was applied to avoid big changes in the topology. It worked as expected, but still need improvements to help to achieve even better topologies. More studies and explorations are necessary to understand how the method would work with different conditions and problems.

6. ACKNOWLEDGEMENTS

This study was funded in part by the Coordenação de Aperfeiçoamento de Pessoal de Nível Superior — Brasil (CAPES) — Finance Code 001 and by the FAPESP (São Paulo Research Foundation) [grant number 2013/08293-7]. We thank the laboratory colleague Breno Vincenzo de Almeida for providing the flood fill algorithm, which was used to identify fluid elements of the topology.

7. REFERENCES

Chen, F., Xu, W., Zhang, H., Wang, Y., Cao, J., Wang, M.Y., Ren, H., Zhu, J. and Zhang, Y.F., 2018. "Topology optimized design, fabrication, and characterization of a soft cable-driven gripper". In *IEEE ROBOTICS AND AUTOMATION LETTERS*. IEEE.

Cunha, D.C., 2019. *Otimização Topológica na Concepção de Fluidoatuadores Celulares*. Master's thesis, Faculdade de Engenharia Mecânica - Universidade Estadual de Campinas, Campinas.

de Souza, E.M. and Silva, E.C.N., 2020. "Topology optimization applied to the design of actuators driven by pressure loads". *Structural and Multidisciplinary Optimization*, Vol. 61, No. 5, pp. 1763–1786.

Frecker, M.I., Ananthasuresh, G.K., Nishiwaki, S., Kikuchi, N. and Kota, S., 1997. "Topological synthesis of compliant mechanisms using multi-criteria optimization". *Journal of Mechanical Design*.

Howell, L.L., Magleby, S.P. and Olsen, B.M., 2013. *Handbook of Compliant Mechanisms*. Wiley.

Huang, X. and Xie, Y.M., 2010. *Evolutionary Topology Optimization of Continuum Structures: Methods and Application*. Wiley.

Kumar, P., Frouws, J.S. and Langelaar, M., 2020. "Topology optimization of fluidic pressure-loaded structures and compliant mechanisms using the Darcy method". *Structural and Multidisciplinary Optimization*, Vol. 61, pp. 1637–1655.

Kumar, P. and Langelaar, M., 2021. "On topology optimization of design-dependent pressure-loaded three-dimensional structures and compliant mechanisms". *International Journal for Numerical Methods in Engineering*, Vol. 122, No. 9, pp. 2205–2220.

Kumar, P. and Langelaar, M., 2022. "Topological synthesis of fluidic pressure-actuated robust compliant mechanisms". *Mechanism and Machine Theory*, Vol. 174, p. 104871.

Li, Y., 2014. *Topology optimization of compliant mechanisms based on the BESO method*. Ph.D. thesis, School of Civil, Environmental and Chemical Engineering - RMIT University.

Liu, S., Li, Q., Chen, W., Tong, L. and Cheng, G., 2015. "An identification method for enclosed voids restriction in manufacturability design for additive manufacturing structures". *Frontiers of Mechanical Engineering*, Vol. 10, pp. 126–137.

Lopes, H.N., Cunha, D.C., Pavanello, R. and Mahfoud, J., 2022. "Numerical and experimental investigation on topology optimization of an elongated dynamic system". *Mechanical Systems and Signal Processing*, Vol. 165, p. 108356.

Lu, Y. and Tong, L., 2021. "Topology optimization of compliant mechanisms and structures subjected to design-dependent pressure loadings". *Structural and Multidisciplinary Optimization*, Vol. 63, pp. 1889–1906.

Madrid, C.M.P., 2016. *Otimização Topológica Bidirecional Evolucionária para o Projeto de Mecanismos Flexíveis usando um Enfoque Multi-critério*. Master's thesis, Faculdade de Engenharia Mecânica - Universidade Estadual de Campinas.

Xie, Y.M. and Steven, G.P., 1992. "Shape and layout optimization via an evolutionary procedure". In *Proceedings of the international conference on computational engineering science*.

Yang, X.Y., Xie, Y.M. and Steven, G., 2005. "Evolutionary methods for topology optimisation of continuous structures with design dependent loads". *Computers & structures*, Vol. 83, No. 12-13, pp. 956–963.

Yap, H.K., Ng, H.Y. and Yeow, C.H., 2016. "High-force soft printable pneumatics for soft robotic applications". *Soft Robotics*, Vol. 3, No. 3, pp. 144–158.

Zhu, B., Zhang, X., Zhang, H., Liang, J., Zang, H., Li, H. and Wang, R., 2020. "Design of compliant mechanisms using continuum topology optimization: A review". *Mechanism and Machine Theory*, Vol. 143, p. 103622.

8. RESPONSIBILITY NOTICE

The authors are solely responsible for the printed material included in this paper.